Relationship between the Nanostructures and the Optical Properties of CeO_2 Thin Films

Roberta G. Toro, Graziella Malandrino,* and Ignazio L. Fragalà*

Dipartimento di Scienze Chimiche, Università di Catania, and INSTM, UdR Catania, Viale A. Doria 6, 95125 Catania, Italy

Raffaella Lo Nigro

IMM, sezione di Catania, CNR, Stradale Primosole n 50, 95121 Catania, Italy

Maria Losurdo* and Giovanni Bruno

Istituto di Metodologie Inorganiche e dei Plasmi, IMIP-CNR, and INSTM, UdR Bari, via Orabona 4, 70126 Bari, Italy

Received: May 4, 2004; In Final Form: September 7, 2004

CeO_2 nanostructured thin films have been deposited on $Al_2O_3(1-102)$ and $TiO_2(001)$ single-crystal substrates through metal−organic chemical vapor deposition (MOCVD) using the Ce(III) 1,1,1,5,5,5-hexafluoro-2,4-pentanedionato diglyme adduct ($Ce(hfa)_3$·diglyme). Structural and morphological characterizations have been carried out by X-ray diffraction pattern (XRD), atomic force microscopy (AFM), and scanning electron microscopy (SEM) measurements. It has been found that the deposition temperature and the lattice mismatch with the substrate have a strong impact on the film nanostructure. X-ray diffraction patterns of samples grown at low deposition temperature point to the formation of ⟨100⟩ oriented CeO_2 films, while films deposited at higher deposition temperatures have ⟨111⟩ texture. Furthermore, SEM cross section images clearly point to relevant effects of deposition temperatures both on the structural alignment of CeO_2 grains as well as on the film/substrate interfaces. Spectroscopic ellipsometric measurements provide a suitable rationalization of correlations between nanostructures and optical properties of the CeO_2 films. Moreover, combination of SEM and spectroscopic ellipsometric measurements provide an in-depth interpretation of growth modes.

Introduction

Among oxides, the cubic CeO_2 phase (fluorite) has long been considered one of the most promising materials because of the high refractive index, good transmission in the visible and infrared regions, strong adhesion, and high stability against mechanical abrasion, chemical attack, and high temperatures. All these desirable properties have rendered CeO_2 films widely used as optical coatings,[1] supports of metals for catalytic oxidation reactions,[2,3] stable capacitors in silicon-on-insulator structures[4−6] and as a buffer layer for high-temperature superconductor (HTS) thin films.[7,8] In fact, the growth of high quality HTS thin films often requires intermediate buffer layers to prevent any chemical interaction with the substrate. Suitable buffer layers must have, in addition, appropriate lattice constants in order to improve the *c*-axis alignment of HTS films, which represents the most outstanding issue to reach higher current density values.

In this context, CeO_2 is a promising candidate since its fluorite structure ($a = 5.411$ Å) favors a good in-plane alignment of HTS perovskite films having the (001) unit cell 45° rotated in the (100) CeO_2 plane. The efficacy of CeO_2 buffer layers has been proved on a wide range of technical substrates, such as $Al_2O_3(1-102)$, MgO(100), and YSZ(100) (yttria stabilized zirconia), that are currently used to fabricate superconducting microwave components (e.g., filters, strip-line resonators).[9−12]

CeO_2 thin films have been grown by several techniques involving both physical and chemical methods.[13−18] However, in the past few decades the metalorganic chemical vapor deposition (MOCVD) technique has been proved to be a suitable choice for the growth of ceramic thin films for numerous applications in solid-state electronic devices. In particular, we have recently reported on the unique example of CeO_2 thin films grown on TiO_2 substrate.[19] There is, in fact, interest for the fabrication of HTS passive filters on TiO_2 rutile substrates, because of the very low dielectric tangent loss and high thermal conductivity of rutile.[20] CeO_2, however, belongs to a different space group than TiO_2, and in particular, they possess two different crystal structures, fcc-fluorite and tetragonal symmetry, respectively. Therefore, the lattice mismatch $CeO_2(100)$/$TiO_2(001)$ is about 17%. Note that a considerably better matching is found with $Al_2O_3(1-102)$ substrate, commonly used for the growing of highly epitaxial ⟨100⟩ CeO_2 films, with mismatch values of 5.7% and 12% along the *a* and *c* directions, respectively.

In earlier studies,[19−22] we have devoted great efforts to understanding the role played either by the lattice mismatch or by deposition conditions on the in-plane and out-of-plane epitaxy of CeO_2 films. In particular, results have been rationalized in terms of surface mobility and lattice matching.

As far as the optical properties of CeO_2 films are concerned, it has been shown that the refractive index and absorption of CeO_2 films are strongly dependent on deposition parameters

* Corresponding authors. E-mail: (G.M.) gmalandrino@dipchi.unict.it; (I.L.F.) lfragala@dipchi.unict.it; (M.L.) cscpml18@area.ba.cnr.it.

10.1021/jp048083j CCC: $27.50
Published on Web 09/29/2004

that, in turn, induce different orientations and O-deficiencies in the films.[23,24]

In this general perspective, the present study focuses on correlations between microstructures and optical properties of epitaxial CeO_2 thin films grown using MOCVD on two different single crystal, $Al_2O_3(1-102)$ and $TiO_2(001)$, substrates. The heteroepitaxy and quality of CeO_2 films depend critically on the lattice mismatch between film and substrate. The influence of the substrate lattice parameters and of the deposition conditions on the nature of both film/substrate interface and initial layers, has been analyzed. Spectroscopic ellipsometric (SE) and scanning electron microscopy (SEM) data provide evidence of interrelations between optical properties and structural changes due to processing conditions and substrates.

Experimental Section

Film Synthesis and Characterization. CeO_2 films were prepared in a reduced pressure horizontal hot-wall MOCVD reactor from the $Ce(hfa)_3$·diglyme [Hhfa = 1,1,1,5,5,5-hexafluoro-2,4-pentanedione, diglyme = bis(2-methoxyethyl) ether] precursor.[25] Deposition experiments were carried out as described elsewhere.[19] $Al_2O_3(1-102)$ and $TiO_2(001)$ substrates were purchased from Crystal GmbH.

Surface morphology was examined using a LEO Iridium 1450 scanning electron microscope (SEM). $\theta-2\theta$ X-ray diffraction (XRD) patterns and ω-scans were recorded on a Bruker-AXS D5005 $\theta-\theta$ X-ray diffractometer, using Cu Kα radiation (40 kV and 30 mA). A four circle Bruker-AXS D5005 X-ray diffractometer was used to characterize the in-plane grain alignment of CeO_2 films.

The optical properties of the films, namely, the complex refractive index, $N = (n + ik)$ (where n is the real refractive index and k is the extinction coefficient, which is proportional to the absorption coefficient $\alpha = 4\pi k/\lambda$) and the dielectric function $\epsilon = \epsilon_1 + i\epsilon_2 = N^2$ were determined using spectroscopic ellipsometry (SE). SE spectra of the real, $\langle\epsilon_1\rangle$, and imaginary, $\langle\epsilon_2\rangle$, parts of the complex pseudodielectric function were measured in the 1.5−5.5 eV energy range using a phase modulated spectroscopic ellipsometer (UVISEL, Jobin-Yvon) at multiple angle of incidence in the range 55−75°.

Background of the Spectroscopic Ellipsometric Measurements. Spectroscopic ellipsometry is a nondestructive and noninvasive optical technique for determining structural and optical properties of surfaces and thin films. If linearly polarized light of a known orientation is reflected at oblique incidence from a surface then the reflected light is elliptically polarized. The shape and orientation of the ellipse depend on the angle of incidence, the direction of the polarization of the incident light, and the reflection properties, which are related to the complex refractive index and dielectric function of the surface/film.

Ellipsometry measures the changes in the polarization state of linearly polarized light when it is reflected from a sample. In particular, it measures the relative phase change, Δ, and the relative amplitude change, Ψ, of the polarized light beam introduced by reflection from the surface, as schematized in Figure 1 for a two phase substrate/ambient case. From the ellipsometric parameters Ψ and Δ, the complex reflectance ratio $\rho = \tan\Psi \exp(i\Delta)$ is measured.[26] ρ gives the ratio between the s-polarized (**E**-field polarized perpendicular to the plane of incidence) and p-polarized (**E**-field polarized parallel to the plane of incidence) light reflected off the surface of interest ($\rho = (E_{rp}/E_{ip})/(E_{rs}/E_{is}) = r_p/r_s$). These are measurable quantities that relate directly to Fresnel's reflection coefficients,

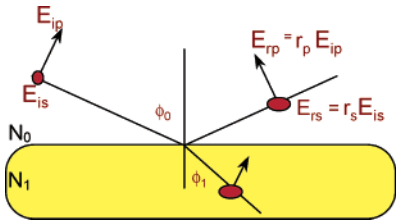

Figure 1. Scheme for reflection of linearly polarized light at the interface between a medium with refractive index N_1 and the ambient with refractive index N_0. r_p and r_s are the Fresnel reflection coefficient for the p (parallel) and s (perpendicular) components of the light beam. E_{ip} and E_{is} indicate the electric vector of the p (parallel) and s (perpendicular) components of the incident light beam, while E_{rp} and E_{rs} are the corresponding for the reflected light beam.

r_p and r_s, which can then provide information on the complex index of refraction and on the complex dielectric function $\epsilon = \epsilon_1 + i\epsilon_2 = N^2 = (n + ik)^2$, by the expression

$$\langle\epsilon\rangle = \epsilon_0 \tan^2\phi\left[1 + \sin^2\phi\frac{(1-\rho)^2}{(1+\rho)^2}\right] \quad (1)$$

where ϵ_0 is the dielectric function of the ambient and ϕ is the angle of incidence.

Modeling of CeO_2 Ellipsometric Spectra. The dielectric and optical properties of a semiconductor oxide are correlated to its energy-band structure, i.e., the energy-dependent dielectric function $\epsilon(E)$ of a semiconductor can be expressed by contributions of electronic transitions from valence electrons. Electronic transitions are responsible for all the structures/peaks in the optical functions. The contribution of valence to conduction band (VB-to-CB) transitions can be taken into account by a combination of oscillators, each oscillator representing an electronic transition, whose parameters are the resonance energy, the strength, and the damping factor.

The CeO_2 has an onset of absorption due to electronic transitions in the visible range. The two main transitions involved in the absorption of CeO_2 films in the visible-UV range are from the highest occupied valence 2p oxygen band into empty 4f states of cerium at about 4 eV (O 2p → Ce 4f) and from the 2p band into the d conduction band at about 9 eV (O 2p → Ce 5d).

Therefore, two Tauc−Lorentz oscillators[27] (2-TL) that take into account the contribution of the main electronic 2p → 4f and 2p → 5d interband transitions to the complex dielectric function, $\epsilon(E) = \epsilon_1(E) + i\epsilon_2(E)$ were used to describe the energy, E, dispersion of the optical properties of the nanocrystalline CeO_2 films.

According to the 2-TL model, the extinction coefficient, k, is given by

$$k(E) = \left(\sum_{i=1}^{2}\frac{A_i}{E^2 - B_i E + C_i}\right)(E - E_0)^2$$

and the refractive index is given by

$$n(E) = \sqrt{\epsilon_\infty} + \sum_{i=1}^{2}\frac{B_{0i}E + C_{0i}}{E^2 - B_i E + C_i}$$

where A_i, B_i, C_i are the fit parameters (related to the resonance energy, strength and damping factor; B_{0i} and C_{0i} are related to A_i, B_i, C_i according to equations reported in ref 27. E_0 is the

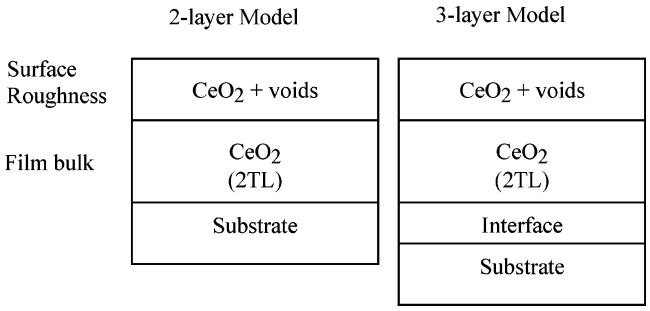

Figure 2. Two-layer and three-layer models used for the analysis of the ellipsometric spectra of the CeO_2 films.

fundamental band gap and ϵ_∞ is the high-frequency dielectric constant, which are also fit parameters.

Furthermore, the structure of the film, i.e., nonhomogeneity or a layered structure because of the presence of a film/substrate interface layer and surface roughness, is considered through layered models. A two-layer model, substrate/CeO_2/CeO_2+voids/ambient, sketched in Figure 2, where the bottom layer represents a dense region of the film and the top layer represents the surface roughness, was used for modeling the SE spectra. For some samples, an additional substrate/film interface layer (the three-layer model in Figure 2) applied, being the thickness of the layers another fit parameter.

Results and Discussion

Structural Properties. Our previous reports[19−22] have clearly demonstrated the efficacy of the $Ce(hfa)_3$·diglyme adduct to act as Ce source for the deposition of high quality CeO_2 oriented films on both conventional and non conventional (i.e metal alloy, Hastelloy C276) substrates. One of the major advantages of the $Ce(hfa)_3$·diglyme precursor is associated with the rather low deposition temperature needed to grow CeO_2 films. The CeO_2 films have been deposited on both the $Al_2O_3(1-102)$, and $TiO_2(001)$ substrates in the 450−900 °C temperature range. To obtain deep insights on relations between microstructure and optical properties as well as to understand the influence of the substrate lattice parameters on the initial layers and on film/substrate interface, three representative samples have been selected, as case studies of interest for our investigation.

The $\theta-2\theta$ XRD spectra of films deposited on $Al_2O_3(1-102)$ at 450 °C and on $TiO_2(001)$ at 600 and 900 °C are shown in Figure 3. In the case of films grown on $Al_2O_3(1-102)$ there is evidence of purely ⟨100⟩ oriented CeO_2 films (Figure 3a). Films deposited on $TiO_2(001)$ at 600 °C are also ⟨100⟩ oriented (Figure 3b). Some differences become, however, evident by recording the (200) CeO_2 reflection rocking curve since full width half maximum (fwhm) values are indicative of out-of-plane misalignments of CeO_2 films. Thus, in the case of the $CeO_2(100)/TiO_2(001)$ system, the fwhm value (∼4.8°) observed at 600 °C (inset in Figure 3b) is greater than the value (fwhm = 2.5°) measured for CeO_2 films on $Al_2O_3(1-102)$ (inset in Figure 3a) substrates. The observed difference is mainly due to the larger mismatch between $CeO_2(100)$ film and $TiO_2(001)$ substrate (17%) than in the case of CeO_2/Al_2O_3 system.

The increase of the deposition temperature up to 900 °C causes a prevalent ⟨111⟩ texturing in CeO_2 films grown on $TiO_2(001)$ substrates (Figure 3c). In this case, the (111) rocking curve fwhm values are better (∼1°) than in the case of $CeO_2(100)$ oriented films deposited at lower temperature.

A better insight into the epitaxial relations between CeO_2 films on $Al_2O_3(1-102)$ and $TiO_2(001)$ substrates has been obtained from X-ray φ scans (Figure 4). In the case of ⟨100⟩

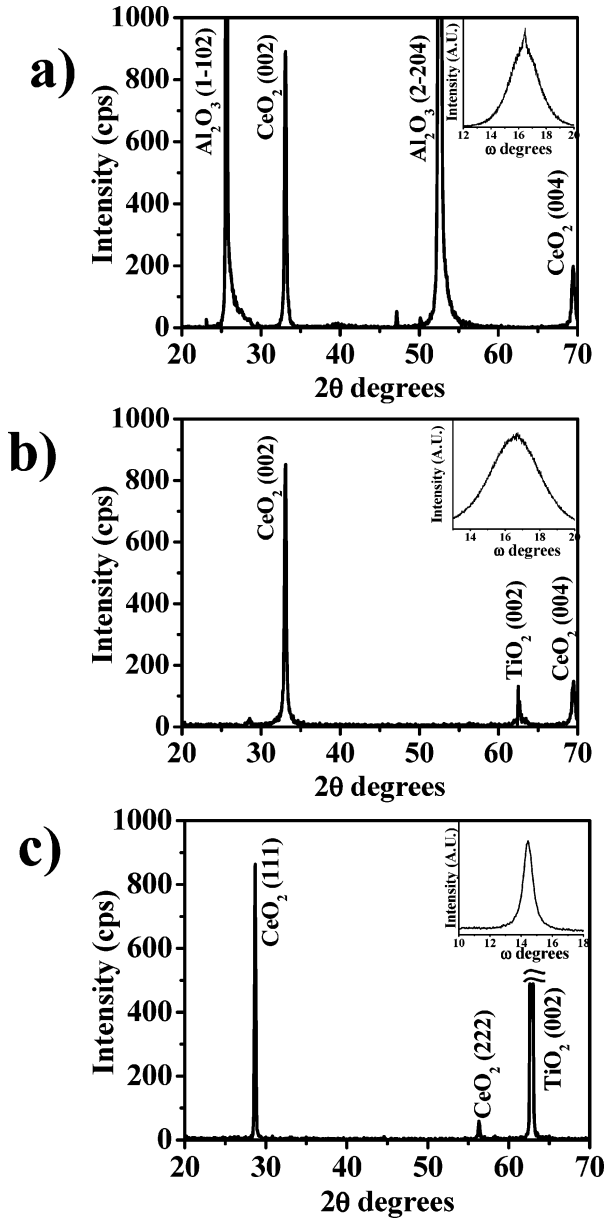

Figure 3. $\theta-2\theta$ scans of (a) a ⟨100⟩ CeO_2 film deposited at 450 °C on (1−102) Al_2O_3, of (b) a ⟨100⟩ CeO_2 film deposited at 600 °C on (001) TiO_2, and of (c) a ⟨111⟩ CeO_2 film deposited at 900 °C on (001) TiO_2. Inserts show the ω-scans for the (200) reflection in the case of ⟨100⟩ CeO_2 films, and for the (111) reflection in the case of ⟨111⟩ oriented CeO_2 films.

CeO_2 samples on Al_2O_3 the φ scan has been recorded by using the (111) reflection ($2\theta = 28.54°$) as a pole. The two maxima observed at $\psi = 54.75°$ in the 0−180° φ range clearly point to epitaxial growth of $CeO_2(100)$ films on $Al_2O_3(1-102)$ substrates since the two peaks, spaced by $\varphi = 90°$, unequivocally point to the 4-fold symmetry of the fcc system.

The $CeO_2(100)$ film deposited at 600 °C on $TiO_2(001)$ does not show any in-plane texturing, and as a consequence the φ scan consists of a flat line. A different behavior has been found for the $CeO_2(111)$ oriented film. In this case, the φ scan recorded using the (200) reflection ($2\theta = 33.09°$) as a pole consists of 6 peaks repeated every 30°. This peculiar trend points to an effective in-plane texturing, associated with grain twinning. Thus, the deposition temperature strongly affects the structural characteristic of the deposited films. A detailed description of the in-plane alignment of CeO_2 films grown on rutile substrate has been already reported elsewhere.[19]

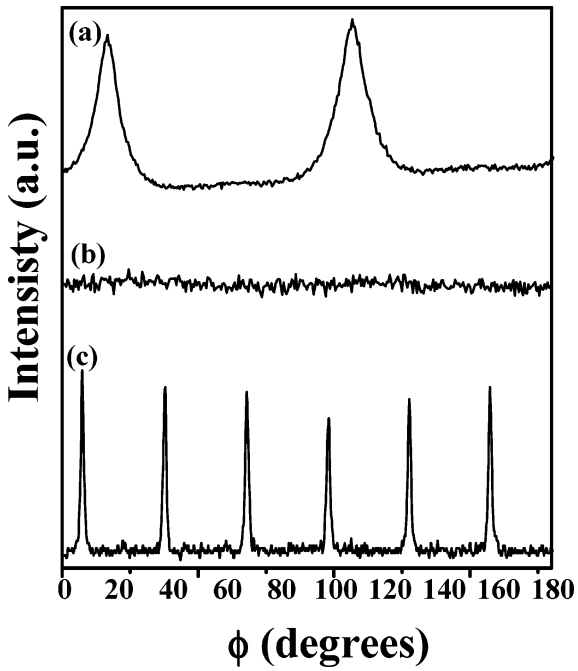

Figure 4. Φ-scans using the (111) or (200) CeO_2 reflection as pole for cerium dioxide films: (a) ⟨100⟩ CeO_2 film deposited at 450 °C on (1−102) Al_2O_3; (b) ⟨100⟩ CeO_2 film deposited at 600 °C on (001) TiO_2; (c) ⟨111⟩ CeO_2 film deposited at 900 °C on (001) TiO_2.

The grain morphology has been examined by atomic force microscopy (AFM). Figure 5 shows typical AFM images of surfaces of CeO_2 films with different microstructures deposited on both Al_2O_3 and TiO_2 substrates. The corresponding line profiles are also shown in Figure 5. The CeO_2(100) films show quite similar morphologies. Nevertheless, CeO_2(100)/Al_2O_3 samples have well shaped grains 100−130 nm wide with abrupt edges pointing to a single-column morphology. Interconnected grains with a more disordered structure are associated with morphologies of the CeO_2(100)/TiO_2 sample. Finally, a different surface morphology, mostly due to grain agglomeration, is detected in CeO_2(111)/TiO_2 samples.

The film morphology has been also investigated by SEM. In particular, SEM cross section images (Figure 6) have been used to evaluate the interface morphological characteristics. Well-defined columnary structures are evident in the case of ⟨100⟩ CeO_2 grown on Al_2O_3(1−102) (Figure 6a). The thickness of these columnar crystallites is about 1500 nm. A sharp interface with the substrate is evident, and the grains grow as single columns very close to each other.

Cross sections of ⟨100⟩ CeO_2 films on TiO_2(001) substrates (Figure 6b,c) show different grain morphologies than the pure columnar growth found in the CeO_2/Al_2O_3(1−102) films. In fact, an initially disordered layer, about 150 nm thick, is evident at the bottom of the columnar grains that are ≈800 nm thick. This points to the relevant role played by the great lattice mismatch between CeO_2 film and (001) TiO_2 substrate.

In the case of ⟨111⟩ CeO_2 oriented film grown on TiO_2(001) substrate at 900 °C SEM micrograph points to a neat interface beneath films with no columnar grains. The thickness of the film is about 1200 nm.

Optical Properties. Figure 7 shows the experimental and calculated spectra of the ellipsometric variables ($I_s = \sin(2\psi)\sin(2\Delta)$ and $I_c = \sin(2\psi)\cos(2\Delta)$) measured at various incidence angles (55, 60, and 65°) for the ⟨100⟩ CeO_2 oriented film grown on TiO_2. The same multiple-incidence angle approach, which improves the accuracy of the fit analysis, has been applied to

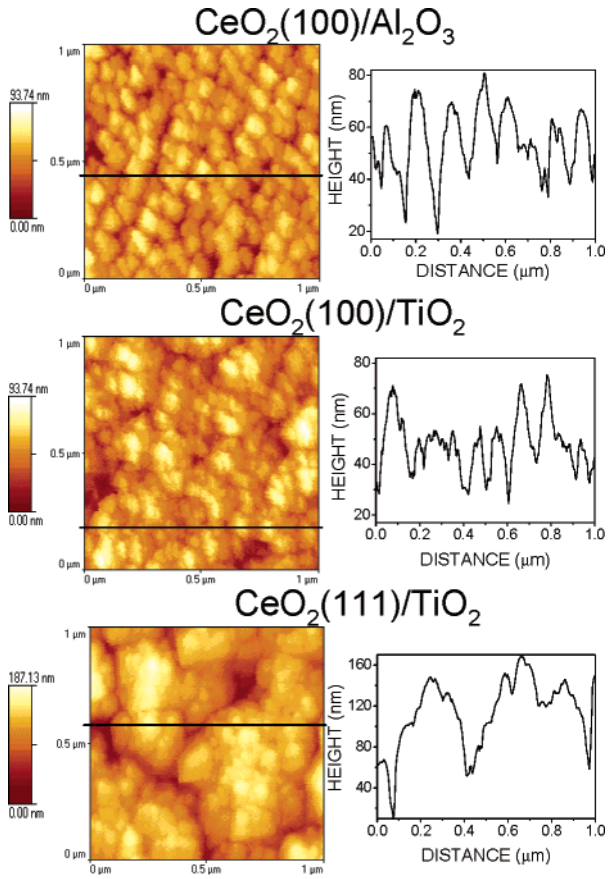

Figure 5. AFM images of microcrystalline CeO_2(100) films grown on Al_2O_3 and TiO_2 and of a CeO_2(111) film grown on TiO_2. Representative line profiles for each image are also shown.

all the investigated samples. Experimental and calculated spectra in terms of the real, $\langle\epsilon_1\rangle = n^2 - k^2$, and imaginary, $\langle\epsilon_2\rangle = 2nk$, parts of the pseudodielectric function (related to the refractive index, n, and extinction coefficient, k) are shown in Figure 8 for the incidence angle of 60° according to the best-fit models sketched at the bottom for the CeO_2 (100) samples grown on both Al_2O_3 and TiO_2 and for the CeO_2(111)/TiO_2 sample. It is worth noting that the best-fit model is a simple two-layer model (film and surface roughness) for the CeO_2(100)/Al_2O_3 and CeO_2(111)/TiO_2 films. In contrast, a three-layer model applies for the CeO_2(100)/TiO_2 system, which is characterized by the presence of a less ordered and less dense (as indicated by the inclusion of voids) TiO_2/CeO_2 interface layer with a thickness of 72 ± 4 nm, in agreement with SEM data (Figure 6). This interface layer is absent in the CeO_2(100)/Al_2O_3 and in the CeO_2(111)/TiO_2 samples, as already observed in the cross-section SEM images. By applying the models in Figure 8 and the 2TL-expression for the description of the CeO_2 optical properties, we derived the spectra of the refractive index, n, and extinction coefficient, k, shown in Figure 9 for the same samples. The main fit parameters, i.e., the high-frequency dielectric constant, ϵ_∞, the main oscillator resonance energy, E_1, and the Tauc-energy gap, E_o, of the investigated films, are reported in Table 1. The value of the high-frequency dielectric constant, ϵ_∞, is an important parameter for evaluation of the film quality and porosity; i.e., the closer the value to that of the single crystal, the better the film quality in terms of order and density. From the two-TL fitting analysis, the value of $\epsilon_\infty = 5.22 \pm 0.19$ is found for the CeO_2(100)/TiO_2 sample in close agreement with that reported for CeO_2 bulk crystal.[28] ϵ_∞ decreases to 4.23 ± 0.18 and to 2.19 ± 0.07 for the CeO_2(100)/

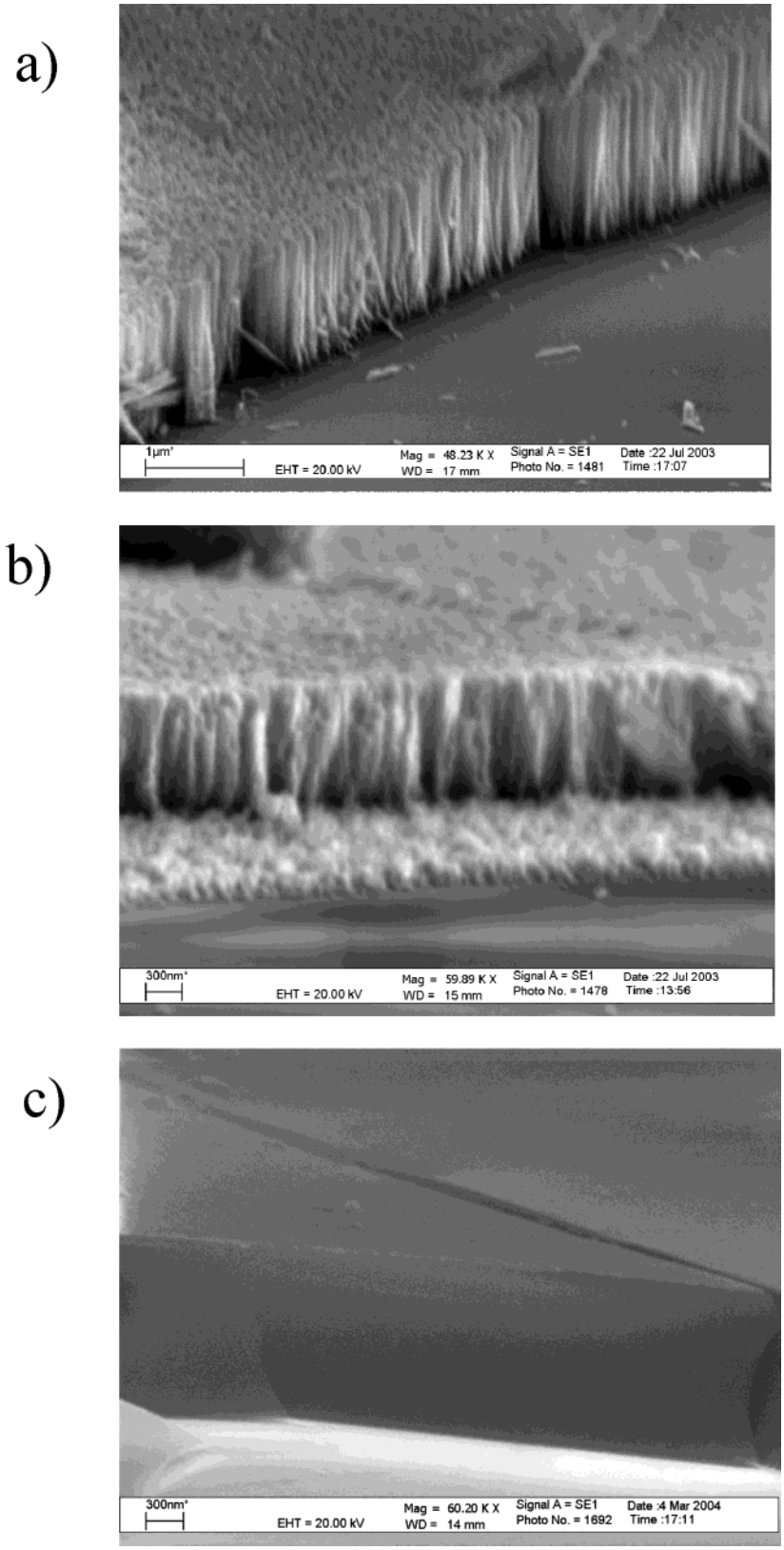

Figure 6. SEM cross-section images of (a) a ⟨100⟩ CeO_2 film deposited at 450 °C on (1−102) Al_2O_3, (b) of a ⟨100⟩ oriented CeO_2 film deposited at 600 °C on (001) TiO_2, and of (c) a ⟨111⟩ CeO_2 oriented film deposited at 900 °C on (001) TiO_2.

Al_2O_3 and the $CeO_2(111)/TiO_2$ samples, respectively. This trend of ϵ_∞ parallels that of the refractive index (Figure 9). The observed difference in the refractive index could mainly be attributed to the film density; i.e., the higher the density and structural order, the higher the refractive index. In particular, although cross-section SEM data show the same columnar structure with a grain diameter of about 100 nm for both $CeO_2(100)$ films on Al_2O_3 and TiO_2 substrates, XRD data point to a higher crystalline order in the case of $CeO_2(100)/Al_2O_3$ films. A similar conclusion can be deduced from AFM microscopy images (Figure 5) showing well-defined single-column grains for the $CeO_2(100)/Al_2O_3$ films and grains much

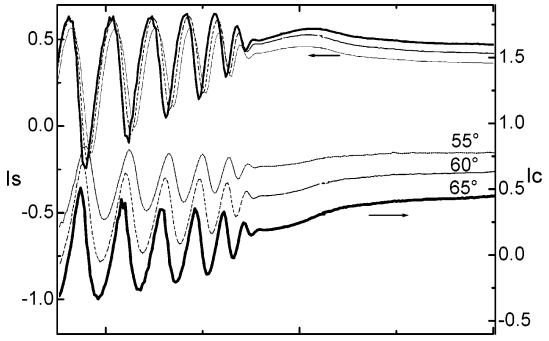

Figure 7. Experimental spectra of the ellipsometric variables $I_s = \sin(2\psi)\sin(2\Delta)$ and $I_c = \sin(2\psi)\cos(2\Delta)$ acquired at incidence angles of 55, 60, and 65°.

TABLE 1: Best-Fit Values for the High-Frequency Dielectric Constant, ϵ_∞, the Main Oscillator Resonance Energy, E_1, and the Tauc-Energy Gap, E_o from the Two-Tauc-Lorentz Parameterization

film	grain size (nm)	ϵ_∞	E_1 (eV)	E_o (eV)
$CeO_2(100)/Al_2O_3$	100	4.23 ± 0.18	3.89 ± 0.03	3.05 ± 0.04
$CeO_2(100)/TiO_2$	100	5.21 ± 0.19	3.65 ± 0.06	3.00 ± 0.05
$CeO_2(111)/TiO_2$	20	2.19 ± 0.07	4.04 ± 0.02	undefined

more interconnected and disordered for $CeO_2(100)/TiO_2$ films. The differently packed microstructures cause different densities and, hence, different spectra of the refractive index. In particular, the higher structural order of the $CeO_2(100)/Al_2O_3$ yields a sharper peak in its *n* and *k* spectra.

In the case of $CeO_2(111)/TiO_2$ films the lower structural order, the smaller grain size (~20 nm) and the different orientation result in the lowest refractive index value.

Information on the structural quality of films can be also achieved from the spectra of the extinction coefficient. In particular, the extinction coefficient spectra (Figure 9) show that the *k* value of the $CeO_2(100)$ films is smaller than 0.01 below 3.1 eV, while for photon energies above 3.1 eV, *k* increases sharply, as expected for a film with sharp band edge profiles without defect states into the band gap or at the band tail. In contrast, an absorption tail, extending to lower photon energies, without an abrupt increase of absorption at the gap is observed for the $CeO_2(111)/TiO_2$ thin film. The absorption tail observed for the $CeO_2(111)/TiO_2$ thin film is due to a high density of defect states introduced in the band gap and originated from the structural disorder. Therefore, the well ordered $CeO_2(100)$ microcrystalline materials have a sharper optical absorption edge and higher optical gap energy than the $CeO_2(111)$ film. In particular, the *k* spectrum of $CeO_2(100)/Al_2O_3$ film has a strong UV absorption, but it is completely transparent in the visible, thus indicating that well ordered microcrystalline $CeO_2(100)$ films are good candidates as UV absorbing materials.

Data in Table 1 show that the maximum of absorption due to the O 2p → Ce 4f transition yields the corresponding oscillator resonance energy at 3.89 ± 0.03 and 3.65 ± 0.06 eV for the $CeO_2(100)/Al_2O_3$ and $CeO_2(100)/TiO_2$ films, respectively. A blue-shift to 4.04 ± 0.02 eV has been found for the resonance energy of the O 2p → Ce 4f transition of the $CeO_2(111)/TiO_2$ film, which can be due to the lower grain size of about 20 nm. This indicates that the oscillator resonance energy from ellipsometric measurements can provide information on the grain size of microcrystalline CeO_2 films.

The optical Tauc-gap energy has also been determined and found to be at 3.00 ± 0.05 and 3.05 ± 0.04 eV for the $CeO_2(100)/Al_2O_3$ and $CeO_2(100)/TiO_2$ films, respectively. These

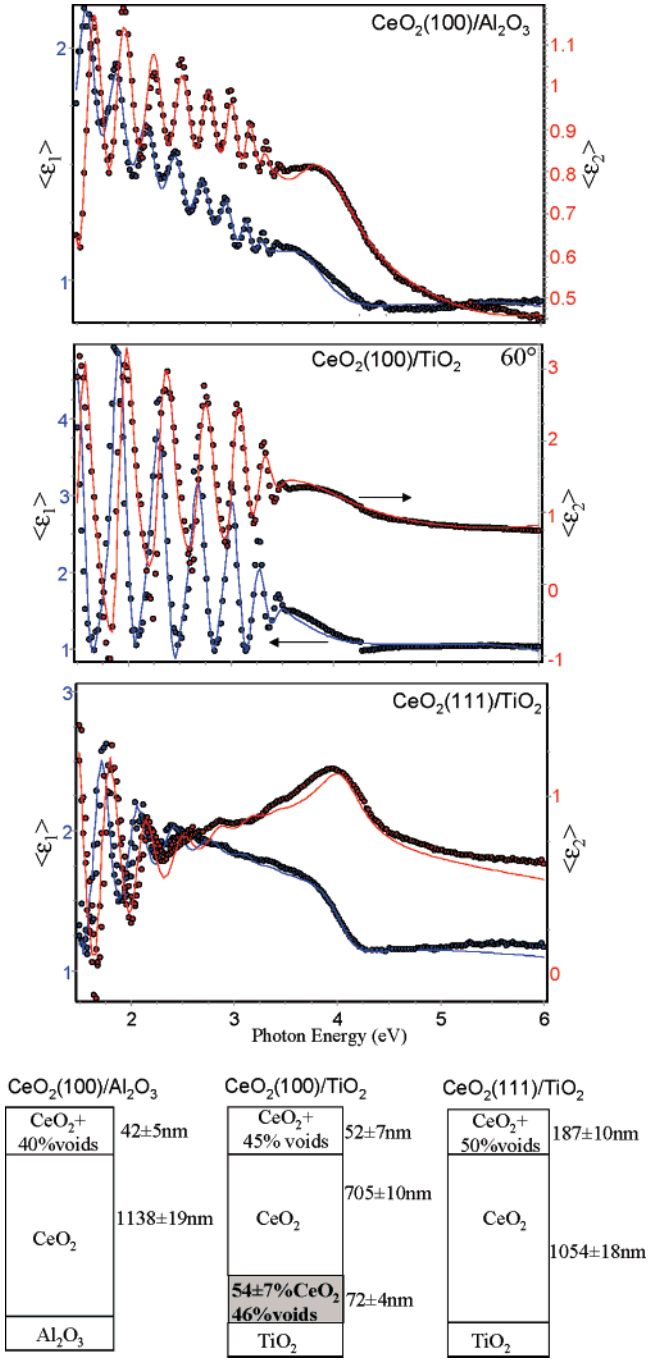

Figure 8. Experimental and calculated spectra of $\langle\epsilon_1\rangle$ and $\langle\epsilon_2\rangle$ for the incidence angle of 60° according to the best-fit model sketched at the bottom for the $CeO_2(100)/Al_2O_3$, $CeO_2(100)/TiO_2$, and $CeO_2(111)/TiO_2$ samples.

values agree well with the indirect gap values of 3.01−3.10 eV reported for fully oxidized crystalline CeO_2 films,[29,30] and this is indicative of the good optical quality of the $CeO_2(100)$ films. In contrast, the $CeO_2(111)$ oriented film deposited at high temperature shows the Urbach tail at low photon energy in the optical absorption, which is caused by defect states in the gap yielding a strong underestimation of the E_g when the TL model is used. The defect states could be due to the higher structural disorder found by the XRD analysis, but also to an oxygen deficiency induced by the higher deposition temperature of 900 °C. In fact, it has been reported that at the outermost surface of nanocrystals both Ce^{4+} and Ce^{3+}coexist, with greater Ce^{3+} quantities upon decreasing the nanocrystal size.[31] Ce^{3+} yields absorption below the gap,[32] and the *k* spectra in Figure 9 show

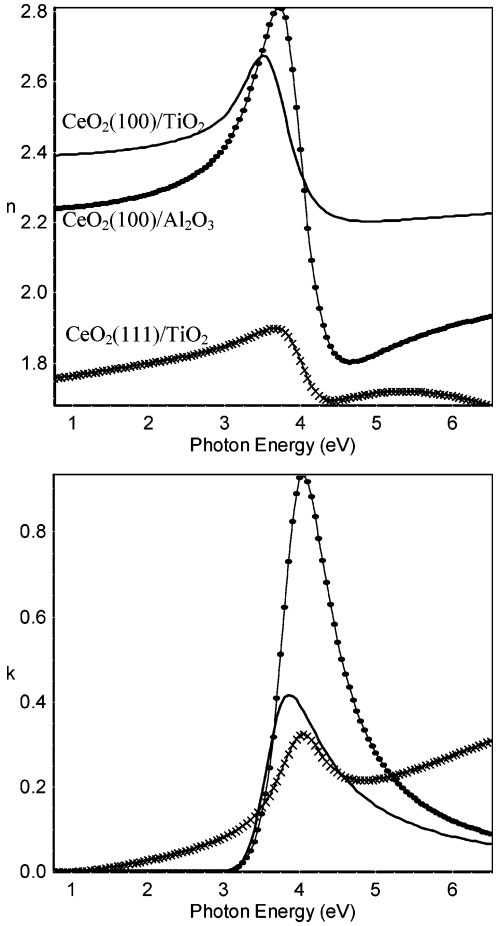

Figure 9. Spectra of the refractive index and extinction coefficient for the $CeO_2(100)/Al_2O_3$, $CeO_2(100)/TiO_2$, and $CeO_2(111)/TiO_2$ samples.

that this absorption tail is present for the sample that also have the lower grain size of about 20 nm. The lower grain size for the $CeO_2(111)/TiO_2$ film also explains the blue-shift found for the resonance energy of the O 2p → Ce 4f transition at 4.04 ± 0.02 eV.

Thus, the combined structural−optical analysis has evidenced that (i) $CeO_2(100)$ films are characterized by a structural order higher than the $CeO_2(111)$ films, (ii) the refractive index is related to film density and structural order, (iii) the oscillator resonance energy is related to the grain size, and (iv) the optical gap is affected by the structural defect states, by the grain size and by the oxygen deficiency.

Growth Model. Ellipsometric measurements and SEM observations both point to a great influence of the lattice parameter mismatch on the structural and morphological characteristics of the CeO_2 film/substrate interface. Present data provide a rationale of the growth mode in both in-plane-epitaxial and nonepitaxial CeO_2 films. Lattice mismatch considerations can be invocated in the case of in-plane oriented $CeO_2(100)||Al_2O_3(1-102)$ and $CeO_2(111)||TiO_2(001)$ films. In particular, the (1−102) Al_2O_3 possesses $a = 4.751$ Å and $c = 12.970$ Å lattice parameters, and by matching five Al_2O_3 unit cells with four CeO_2 unit cells along the a axis, as well as two Al_2O_3 unit cells with five CeO_2 unit cells along the c axis, their lattice mismatches are as small as 8% and 4%, respectively. These values indicate that an epitaxial growth can occur. In the case of the $TiO_2(001)$ substrate, an higher mismatch of 17% would be observed for a cube on cube epitaxial growth. The ⟨100⟩ orientation observed for CeO_2 films grown on TiO_2 at low deposition temperature finds a suitable rationalization within the same model developed for texturing of films deposited via PVD and based on the relationship between differences of surface energies and the elastic energy between grains of different orientations.[33,34] This issue has been deeply addressed in ref 19, together with the reasons of ⟨111⟩ oriented growth on $TiO_2(001)$ substrate. It is interesting to note that when the substrate directly induces the epitaxial growth (⟨100⟩ CeO_2 on $Al_2O_3(1-102)$ and ⟨111⟩ CeO_2 on $TiO_2(001)$), a neat interface occurs as observed by both SEM and ellipsometric data.

On the other hand, interfacial morphologies of CeO_2⟨100⟩ films on $TiO_2(001)$ do not show pure columnar growth and a small disordered layer beneath columnar grains is found in the SEM cross-section. This observation finds counterpart in the three-layer model substrate/CeO_2 interface + voids/CeO_2/CeO_2 + voids/ambient used for modeling the SE spectra of ⟨100⟩ CeO_2 films on $TiO_2(001)$.

These results point to the important role played by the great lattice mismatch between CeO_2 film and (001) TiO_2 substrate.

Conclusions

Nanocrystalline CeO_2 films have been grown on sapphire $Al_2O_3(1-102)$ and rutile $TiO_2(001)$ using MOCVD from the $Ce(hfa)_3$·diglyme precursor.

Effects of both the deposition temperature and the lattice mismatch on the film nanostructure have been investigated by XRD, AFM, and SEM analyses. Spectroscopic ellipsometry has also been used to find correlations between the nanostructure and optical properties of the CeO_2 films. Present data provide an indication that the lattice mismatch with the substrate is crucial for both the microcrystalline order and the optical properties. In particular, the defect density in the gap and the optical absorption in the visible are correlated with the quality of epitaxial films. It has been found that well ordered $CeO_2(100)$ films with an abrupt optical absorption and high visible transparency can be grown at low temperature (450 °C) on $Al_2O_3(1-102)$. This material, is therefore, a good candidate also for optical applications. $CeO_2(100)$ films with a higher high-frequency dielectric constant and higher density have been grown on $TiO_2(001)$ substrates, despite the disordered layer, lying at the substrate/film interface, that accommodates the CeO_2/TiO_2 mismatch.

Acknowledgment. The authors thank the Ministero dell' Istruzione, dell'Università e della Ricerca (MIUR) for financial support.

References and Notes

(1) Netterfield, R. P.; Saintry, W. G.; Martin, P. J.; Sie, S. H. *Appl. Opt.* **1985**, *24*, 2267.

(2) Ratnasamy, P.; Srinivas, D.; Satyanarayana, C. V. V.; Manikandan, P.; Kumaran, R. S. S.; Sachin, M.; Shetti, V. N. *J. Catal.* **2004**, *221*, 455.

(3) Feng, T.; Vohs, J. M. *J. Catal.* **2004**, *221*, 619.

(4) Nishikawa, Y.; Yamaguchi, T.; Yoshiki, M.; Satake, H.; Fukushima, N. *Appl. Phys. Lett.* **2002**, *81*, 4386.

(5) Nishikawa, Y.; Fukushima, N.; Yasuda, N.; Nakayama, K.; Ikegawa, S. *Jpn. J. Appl. Phys.* **2002**, *41*, 2480.

(6) Kang, J.; Liu, X.; Lian, G.; Zhang, Z.; Xiong, G.; Guan, X.; Han, R.; Wang, Y. *Microelectron. Eng.* **2001**, *56*, 191.

(7) Yamada, Y.; Muroga, T.; Iwai, H.; Watanabe, T.; Miyata, S.; Shiohara, Y. *Supercond. Sci. Technol.* **2004**, *17*, S70.

(8) Bhuiyan, M. S.; Paranthaman, M.; Sathyamurthy, S.; Aytug, T.; Kang, S.; Lee, D. F.; Goyal, A.; Payzant, E. A.; Salama, K. *Supercond. Sci. Technol.* **2003**, *16*, 1305.

(9) Nie, J. C.; Yamasaki, H.; Yamada, H.; Nakagava, Y.; Develos-Bagarinao, K. *Supercond. Sci. Technol.* **2003**, *16*, 768.

(10) Edleman, N. L.; Wang, A. C.; Belot, J. A.; Metz, A. W.; Babcock, J. R.; Kawaoka, A. M.; Ni, J.; Metz, M. V.; Flaschenriem, C. J.; Stern, C. L.; Liable-Sands, L. M.; Rheingold, A. L.; Markworth, P. R.; Chang, R. P. H.; Chudzik, M. P.; Kannewurf, C. R.; Marks, T. J. *Inorg. Chem.* **2002**, *41*, 5005.

(11) Taki, K.; Araki, T.; Yamashita, D.; Hirabajashi, I.; Enomoto, Y.; Suzuki, K. *IEEE Trans. Appl. Supercond.* **2003**, *13*, 2687.

(12) Kawagishi, K.; Komoni, K.; Arasawa, S.; Fukutomi, M.; Togano, K. *Physica C* **2000**, *341*, 2405.

(13) Lee, H. Y.; Kim, S. I.; Hong, Y. P.; Lee, Y. C.; Park, Y. H.; Ko, K. H. *Surf. Coat. Technol.* **2003**, *173*, 224.

(14) Golden, T. D.; Wang, A. Q. *J. Electrochem. Soc.* **2003**, *150*, C621.

(15) Mancini, A.; Celentano, G.; Fabbri, F.; Galluzzi, V.; Petrisor, T.; Rufoloni, A.; Varesi, E.; Vannozzi, A.; Rogai, R.; Boffa, V.; Gambardella, U. *Int. J. Mod. Phys. B* **2003**, *17*, 886.

(16) Song, H. Z.; Wang, H. B.; Zhang, J.; Peng, D. K.; Meng, G. Y. *Mater. Res. Bull.* **2002**, *37*, 1487.

(17) Wang, A. C.; Belot, J. A.; Marks, T. J.; Markworth, P. R.; Chang, R. P. H.; Chudzik, M. P.; Kannewurf, C. R. *Physica C* **1999**, *320*, 154.

(18) Belot, J. A.; Wang, A. C.; McNeely, R. J.; Liable-Sands, L.; Rheingold, A. L.; Marks, T. J. *Chem. Vap. Dep.* **1999**, *5*, 65.

(19) Lo Nigro, R.; Toro, R.; Malandrino, G.; Fragalà, I. L. *Chem. Mater.* **2003**, *15*, 1434.

(20) Templeton, A.; Wang, X. R.; Penn, S. J.; Webb, S. J.; Cohen, L. F.; Alford, N. M. *J. Am. Ceram. Soc* **2000**, *83*, 95.

(21) Lo Nigro, R.; Malandrino, G.; Fragalà, I. L. *Chem. Mater.* **2001**, *13*, 4402.

(22) Lo Nigro, R.; Malandrino, G.; Fragalà, I. L. *Mater. Sci. Eng. B* **2003**, *102*, 323.

(23) Guo, S.; Arwin, H.; Jacobsen, S. N.; Jarrendal, K.; Helmerson, U. *J. Appl. Phys.* **1995**, *77*, 5369.

(24) Zheng, S. Y.; Andersson, A. M.; Galdt, F.; Stjerna, B.; Granqvist, C. G. *Appl. Opt.* **1993**, *32*, 6303.

(25) Lo Nigro, R.; Malandrino, G.; Fragalà, I. L.; Benelli, C. *Chem. Vap. Dep.* **2000**, *6*, 233.

(26) Tomkins, H. G. *A User's Guide to Ellipsometry*; Academic Press: San Diego, CA, 1993.

(27) Jellison, G. E.; Modine, F. A. *Appl. Phys. Lett.* **1996**, *69*, 371.

(28) Mochizuki, S. *Phys. Status Solidi B* **1982**, *114*, 189.

(29) Sundaram, K. B.; Wahid, P. *Phys. Status Solidi B* **1990**, *161*, K63.

(30) Hogarth, C. A.; Al-Dhan, Z. T. *Phys. Status Solidi B* **1986**, *137*, K157.

(31) Tsunekawa, S.; Sahara, R.; Kawazoe, Y.; Kasuya, A. *Mater. Trans.* **2000**, *41*, 1104.

(32) Marabelli, F.; Watcher, P. *Phys. Rev. B* **1987**, *36*, 1238.

(33) Machlin, E. S. *Materials Science in Microelectronics*, Gyro: New York, 1995.

(34) Bunshah, R. F.; Blocher, J. M, Jr.; Mattox, D. M.; et al. *Deposition Technologies for Films and Coating*; Noesy Publication: Park Ridge, NY, 1982.